



SOURCE
DATATRANSPARENT
PROCESS

The pseudophosphatase STYX targets the F-box of FBXW7 and inhibits SCF^{FBXW7} function

Veronika Reiterer^{1,2}, Cristina Figueras-Puig², Francois Le Guerroue³, Stefano Confalonieri^{4,5}, Manuela Vecchi^{6,7}, Dasaradha Jalapothu¹, Sandip M Kanse¹, Raymond J Deshaies^{6,7}, Pier Paolo Di Fiore^{4,5,8}, Christian Behrends^{3,9,*}  & Hesso Farhan^{1,2,10,**} 

Abstract

The F-box protein FBXW7 is the substrate-recruiting subunit of an SCF ubiquitin ligase and a major tumor-suppressor protein that is altered in several human malignancies. Loss of function of FBXW7 results in the stabilization of numerous proteins that orchestrate cell proliferation and survival. Little is known about proteins that directly regulate the function of this protein. In the current work, we have mapped the interactome of the enigmatic pseudophosphatase STYX. We reasoned that a catalytically inactive phosphatase might have adopted novel mechanisms of action. The STYX interactome contained several F-box proteins, including FBXW7. We show that STYX binds to the F-box domain of FBXW7 and disables its recruitment into the SCF complex. Therefore, STYX acts as a direct inhibitor of FBXW7, affecting the cellular levels of its substrates. Furthermore, we find that levels of STYX and FBXW7 are anti-correlated in breast cancer patients, which affects disease prognosis. We propose the STYX–FBXW7 interaction as a promising drug target for future investigations.

Keywords breast cancer; Cullin–RING ubiquitin ligase; F-box protein; mass spectrometry; pseudophosphatase

Subject Categories Post-translational Modifications, Proteolysis & Proteomics

DOI 10.15252/emboj.201694795 | Received 17 May 2016 | Revised 11 November 2016 | Accepted 17 November 2016 | Published online 22 December 2016

The EMBO Journal (2017) 36: 260–273

Introduction

Phosphorylation and ubiquitylation are two major post-translational modifications that regulate fundamental cellular processes such as proliferation, growth, and differentiation. Enzymes that catalyze the transfer or removal of ubiquitin and phosphate are the major regulators of these signaling networks. Besides the undoubted importance of these enzymes in cell homeostasis, mounting evidence indicated that pseudoenzymes play prominent roles in regulating signaling pathways. Pseudoenzymes are proteins that contain mutations in the enzyme domain that are predicted to render them catalytically inactive (Reiterer *et al.*, 2014). Despite some advances in the field, pseudoenzymes largely remain enigmatic and much has to be learned about their basic mechanisms of action and their roles in health and disease.

STYX is the archetype pseudophosphatase that belongs to the family of protein tyrosine phosphatases. Within its phosphatase domain, STYX has a glycine residue at position 120 that is responsible for its catalytic inactivity (Wishart & Dixon, 1998; Reiterer *et al.*, 2014). Mutation of G120 to cysteine restores the ability of STYX to dephosphorylate substrates (Reiterer *et al.*, 2013). We showed previously that the pseudophosphatase STYX binds to the mitogen-activated protein kinases ERK1 and ERK2 to modulate their nucleo-cytoplasmic shuttling and biologic activities (Reiterer *et al.*, 2013). However, it is conceivable that pseudophosphatases such as STYX have evolved to regulate proteins beyond kinases.

Cullin–RING ligases (CRLs) are the largest family of ubiquitin ligases and are composed of several subunits: a cullin scaffold, a RING finger protein (RBX1 or RBX2), and a substrate adaptor (Petroski & Deshaies, 2005). The founding member of the CRL family is the SKP1/CUL1/F-box (SCF) complex. In this complex, CUL1 serves as a scaffold and substrate recognition is mediated by one of the ~70 F-box proteins

1 Institute of Basic Medical Sciences, University of Oslo, Oslo, Norway

2 Biotechnology Institute Thurgau, Kreuzlingen, Switzerland

3 Institute of Biochemistry II, Medical School Goethe University, Frankfurt, Germany

4 The FIRC Institute for Molecular Oncology, IFOM, Milan, Italy

5 Molecular Medicine Program, European Institute of Oncology, Milan, Italy

6 Division of Biology and Biological Engineering, California Institute of Technology, Pasadena, CA, USA

7 Howard Hughes Medical Institute, California Institute of Technology, Pasadena, CA, USA

8 Department of Oncology and Hemato-Oncology, University of Milan, Milan, Italy

9 Munich Cluster for Systems Neurology, Ludwig-Maximilians-University Munich, Munich, Germany

10 Department of Biology, University of Konstanz, Konstanz, Germany

*Corresponding author. Tel: +49 89 4400 46509; E-mail: christian.behrends@mail03.med.uni-muenchen.de

**Corresponding author. Tel: +47 228 51233; E-mail: hesso.farhan@medisin.uio.no

(FBPs) (Jin *et al*, 2004). In addition, CUL1 and FBPs are linked via the protein SKP1. Three types of FBPs are known: FBXWs (contain a WD40 domain), FBXLs (contain leucine-rich repeats), and FBXOs (contain diverse types of domains). All FBPs share a conserved region called the F-box, which is the site where the FBP binds to SKP1. FBPs recruit substrates through variable C-terminal protein–protein interaction domains (Jin *et al*, 2004; Petroski & Deshaies, 2005). The large number and variety of FBPs, which are responsible for substrate binding, allows modular organization of the SCF complex and expands substrate specificity. A remarkable feature of FBPs is that they typically interact with their targets in a phosphorylation-dependent manner, thereby offering a link between kinase/phosphatase signaling and ubiquitylation. The FBP binding motifs in substrates are referred to as phosphodegrons because their phosphorylation is a signal for FBP binding, ubiquitin transfer, and subsequent degradation. One of the best-characterized FBPs is FBXW7 (also known as Fbw7, Ago, Cdc4, or Sel10), which was proposed to act as an important tumor-suppressor (Welcker & Clurman, 2008; Cremona *et al*, 2016). FBXW7 controls the levels of several proteins involved in the regulation of cell cycle or of cell growth such as cyclin E, c-myc, mTOR, KLF5, or the Notch intracellular domain (Koepp *et al*, 2001; Oberg *et al*, 2001; Strohmaier *et al*, 2001; Welcker *et al*, 2004; Mao *et al*, 2008; Zhao *et al*, 2010).

In the current work, we mapped the interactome of STYX and found that it binds to several FBPs, including FBXW7. We show that STYX binds to the F-box of FBXW7, thereby uncoupling it from the SCF^{FBXW7} complex and consequently inhibiting its activity. To the best of our knowledge, this is the first demonstration that a SCF complex is regulated by direct protein–protein interaction with an FBP. Furthermore, we find the levels of STYX and FBXW7 to be anti-correlated in breast cancer patients and that patient survival is modulated by disruption of the balance between STYX and FBXW7 levels.

Results

STYX interacts with FBXW7

To determine whether STYX interacts with proteins beyond kinases and phosphatases, we mapped the interactome of this pseudophosphatase. HEK293 cells expressing hemagglutinin (HA)-tagged STYX were lysed and subjected to anti-HA immunoprecipitation and HA peptide elution followed by liquid chromatography coupled with tandem mass spectrometry (LC-MS/MS) on trypsinized immune

complexes. Total spectral counts for each of the unique proteins were processed using the computational Comparative Proteomics Analysis Software Suite (CompPASS) as described previously (Sowa *et al*, 2009; Behrends *et al*, 2010). Several high-confidence interaction partners (HCIPs) were recovered, among them three different FBPs (Fig 1A and Table EV1). In addition, the previously identified putative STYX-interacting protein FBXL12 (Tan *et al*, 2013) was also present in our interactome though below our strict threshold for HCIP determination (Table EV1). We focused on FBPs due to their noticeable enrichment. Among FBPs, FBXW7 has been proposed to act as an important player in tumorigenesis (Welcker & Clurman, 2008; Cremona *et al*, 2016), and therefore, we devoted our efforts to characterize the binary STYX–FBXW7 interaction and its functional consequences.

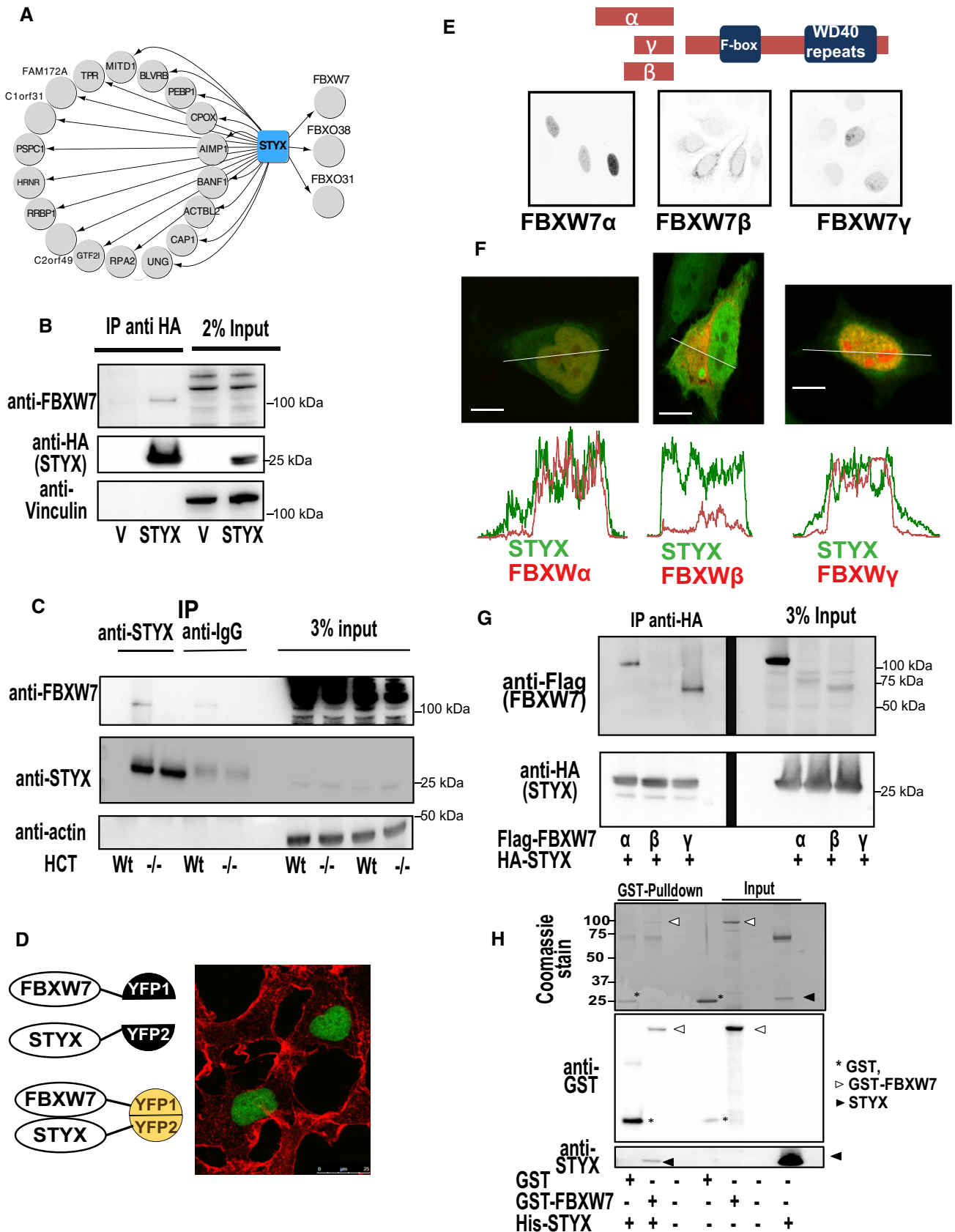
To validate the interactions from our MS experiments, we performed co-immunoprecipitation experiments of HA-tagged STYX with endogenous FBXW7 and found that they readily co-immunoprecipitated (Fig 1B). To test whether both proteins interact at the endogenous level, we used HCT116 cells comparing wild-type cells with an isogenic variant lacking FBXW7. As seen in Fig 1C, endogenous STYX co-immunoprecipitates with endogenous FBXW7. To determine the subcellular location of the interaction, we employed the bimolecular fluorescence complementation (BiFC) assay with severed YFP fragments fused to STYX and FBXW7. We observed that both proteins formed a complex in the nucleus (Fig 1D), which is in line with previous findings that STYX is a predominantly nuclear protein (Reiterer *et al*, 2013).

Three isoforms of FBXW7 exist (α , β , and γ) that differ mainly with respect to their subcellular localization, which is mediated by their divergent N-terminal portions (Fig 1E). All experiments so far were carried out using the FBXW7 α isoform, and therefore, we next investigated whether STYX interacts with all isoforms, or whether it exhibits isoform specificity. FBXW7 α is mainly found in the nucleoplasm, FBXW7 β is mainly cytosolic, and FBXW7 γ is in the nucleolus and the nucleoplasm (Fig 1E). STYX colocalized strongly with FBXW7 α , but only to a very limited extent with FBXW7 β (Fig 1F), which is in line with observation that STYX is mainly found in the nucleus, and to a lesser extent in the cytosol. FBXW7 γ also colocalized with STYX in the nucleoplasm, but not in nucleoli (Fig 1F). In agreement with our colocalization data, STYX co-immunoprecipitated readily with FBXW7 α and FBXW7 γ , but not with FBXW7 β (Fig 1G). Therefore, STYX interacts mainly with the two nuclear isoforms of FBXW7. This specificity likely arises due to spatial reasons.

Figure 1. Interaction of STYX with FBPs.

- High-confidence STYX interaction partners revealed by IP-MS.
- HeLa cells expressing HA-tagged STYX were lysed and subjected to immunoprecipitation against HA followed by immunoblotting as indicated.
- Lysates from wild-type (WT) HCT116 cells or an isogenic line lacking FBXW7 (–/–) were lysed and subjected to immunoprecipitation against STYX or with an irrelevant IgG followed by immunoblotting as indicated.
- YFP–BiFC between STYX and FBXW7 in HeLa cells (green). Cells were co-stained with phalloidin (red). Scale bar = 25 μ m.
- Schematic illustration of the three FBXW7 isoforms (top) and localization of the three Flag-tagged FBXW7 isoforms in HeLa cells by immunofluorescence (bottom).
- HeLa cells expressing Flag-tagged FBXW7 isoforms (red) and YFP-tagged STYX (green) were fixed and stained by immunofluorescence against anti-Flag. Line scans illustrate the degree of the overlap of the staining patterns between STYX and FBXW7 isoforms. Scale bar = 7.5 μ m.
- HeLa cells expressing Flag-tagged FBXW7 isoforms together with HA-tagged STYX were lysed and subjected to immunoprecipitation against HA, followed by immunoblotting as indicated.
- Recombinant 6xHis-tagged STYX was co-incubated with purified GST-tagged FBXW7 or GST followed by GST-pulldown and immunoblotting as indicated. The purified proteins were also separately loaded onto the gel, which was stained with Coomassie.

Source data are available online for this figure.



Finally, we tested whether the interaction between STYX and FBXW7 is direct, or whether it involves a third factor. To this end, we incubated recombinant 6xHis-tagged STYX with recombinant GST-tagged FBXW7. We detected a robust interaction indicating that the STYX–FBXW7 interaction does not require any additional factors (Fig 1H). Altogether, STYX and FBXW7 directly interact and form a complex in the nucleus.

STYX is not a substrate for FBXW7

We next asked what is the functional consequence of the interaction between STYX and FBXW7. We first tested whether STYX is a substrate for this FBP. We silenced FBXW7 using siRNA (Fig 2A) and determined the protein level of STYX, but were unable to observe any detectable effect on the levels of this pseudophosphatase (Fig 2B). To further support this finding, we compared the turnover rate of the well-characterized FBXW7 substrate c-myc in HCT116 cells comparing wild-type cells with a FBXW7^{-/-} isogenic cell line. The decay half-time of c-myc in wild-type cells was in range of 30 min, but was substantially prolonged in FBXW7^{-/-} cells (Fig 2C). Contrarily, STYX was considerably more stable than c-myc and was not affected by the presence or absence of FBXW7 to any detectable extent (Fig 2C). We next overexpressed FBXW7 in HCT116^{FBXW7^{-/-}} cells and observed a marked drop in the levels of c-myc, which is expected for a substrate of FBXW7. However, the levels of STYX did not change in response to FBXW7 overexpression (Fig 2D). Taken together, we conclude that STYX is unlikely to be a substrate for FBXW7.

STYX affects the levels of FBXW7 substrates

Because STYX does not seem to be a substrate of FBXW7, we tested the alternative possibility, namely that STYX regulates the function of FBXW7 and therefore monitored the levels of substrates of this FBP. We first tested whether STYX regulates the levels of c-myc. Knockdown of STYX resulted in a drop in the protein levels of c-myc (Fig 3A and Appendix Fig S1A), but not in its mRNA levels (Fig 3B), indicating that the regulation occurs post-transcriptionally. The effect of STYX on c-myc levels was dependent on FBXW7, because co-depletion of STYX and FBXW7 restored the levels of c-myc back to control levels (Fig 3A). Next, we examined the effect of STYX on another FBXW7 substrate cyclin E (Inuzuka *et al*, 2011; Wertz *et al*, 2011). As in the case of c-myc, the levels of cyclin E were lower in STYX-depleted cells (Fig 3C). These findings indicate that STYX acts as a negative regulator of FBXW7. We also tested whether overexpression of STYX would affect the levels of the FBXW7 substrate c-myc. We overexpressed STYX in HeLa cells and observed that this resulted in a marked increase in basal protein levels of c-myc (Fig 3E). We also followed the protein abundance of c-myc in cycloheximide chase experiments and found that STYX overexpression improves the stability of c-myc (Fig 3D and E). The same was observed for another FBXW7 substrate, MCL1 (Fig 3D and E).

STYX interacts with the F-box of FBXW7

Next, we sought to dissect how STYX regulates the function of FBXW7. We envisaged three possible explanations for this functional interaction. STYX might either regulate the levels of FBXW7,

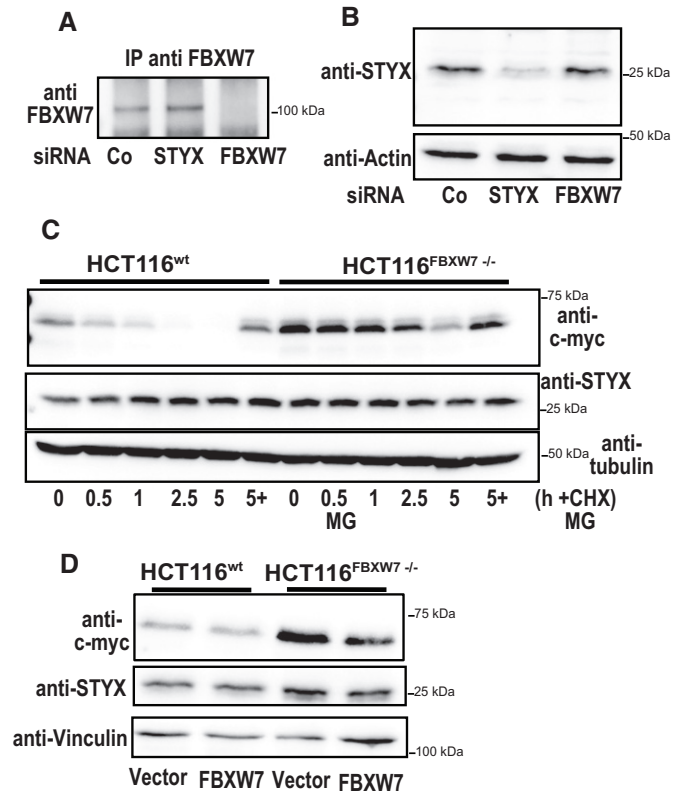


Figure 2. STYX is not a substrate for FBXW7.

- A HeLa cells were transfected with the indicated siRNA. After 72 h, cells were lysed and FBXW7 was immunoprecipitated followed by immunoblotting against FBXW7 to determine knockdown efficiency.
- B HeLa cells were transfected with the indicated siRNA. After 72 h, cells were lysed and immunoblotted as indicated.
- C Wild-type (wt) and FBXW7 knockout (FBXW7^{-/-}) HCT116 cells were treated with cycloheximide (CHX) for the indicated time points. MG indicates treatment with MG132 in parallel to CHX. Cells were lysed and immunoblotted as indicated.
- D Wild-type (wt) and FBXW7 knockout (FBXW7^{-/-}) HCT116 cells were transfected with an empty vector or with a plasmid encoding FBXW7. After 24 h, cells were lysed and immunoblotted as indicated.

or it might compete with substrates for binding to FBXW7, or STYX might disable FBXW7 from inclusion into the SCF complex by binding to the F-box domain.

The effect of STYX depletion on FBXW7 substrates seems unlikely to be due to an increase in the levels of this FBP (Appendix Fig S1B). Dimerization of FBXW7 was shown to regulate its ability to degrade substrates (Welcker & Clurman, 2007). Therefore, we tested whether STYX regulates FBXW7 dimerization. HeLa cells expressing YFP- and HA-tagged FBXW7 were additionally transfected with STYX. Immunoprecipitation of HA-FBXW7 brought down YFP-FBXW7 (Appendix Fig S1C), and overexpression of STYX did not affect the ability of FBXW7 to dimerize.

Next, we tested whether STYX interacts with the substrate-binding domain or with the F-box in FBXW7. We generated a mutant of FBXW7 lacking the F-box (Δ FB in Fig 4A). Substrate binding can be affected by replacing arginine 456 by cysteine in the WD40 repeat domain (displayed as RC in Fig 4A), creating a

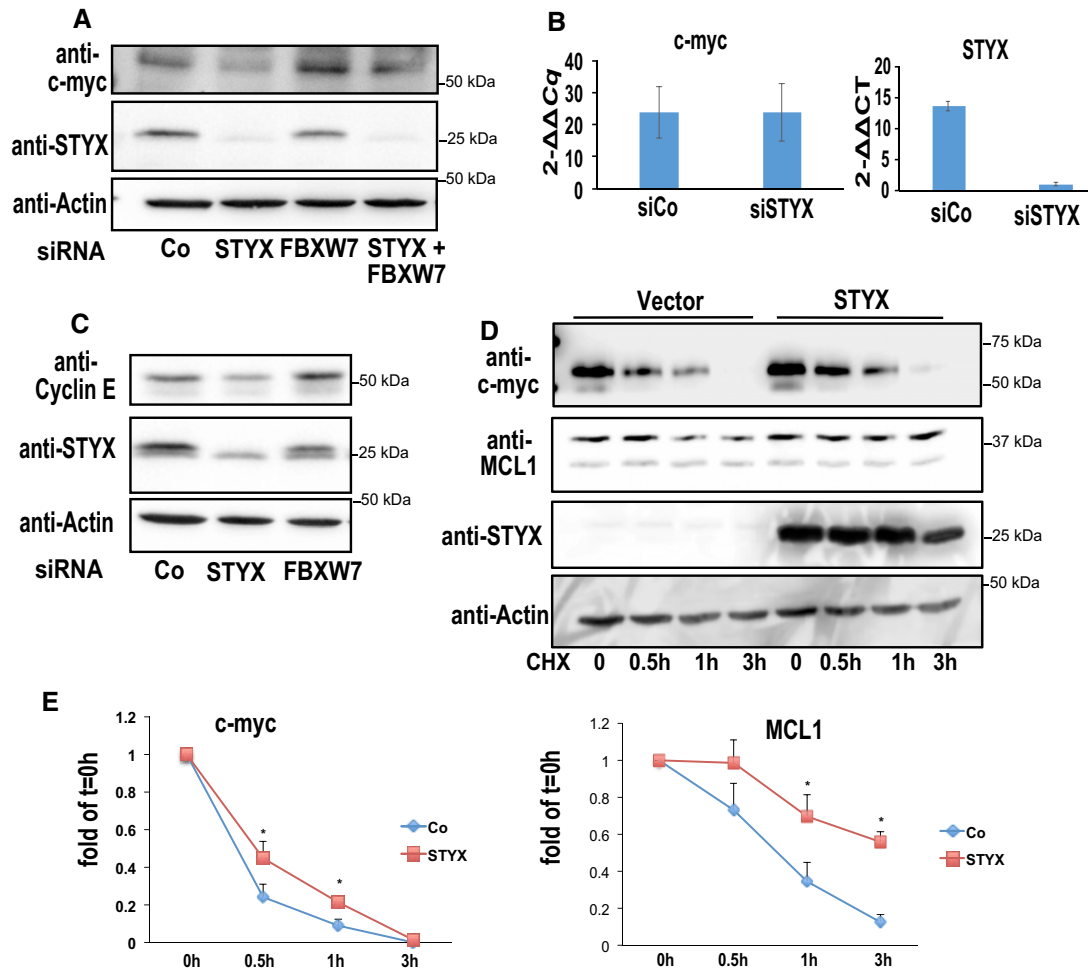


Figure 3. STYX regulates the cellular levels of FBXW7 substrates.

- A HeLa cells were transfected with siRNAs against STYX (siSTYX), FBXW7 (siFBXW7), or with a non-targeting control siRNA (siCo). After 72 h, cells were lysed and subjected to immunoblotting as indicated.
- B HeLa cells transfected siRNAs against STYX (siSTYX), or with a non-targeting control siRNA (siCo). After 72 h, mRNA was extracted and quantitative RT-PCR was performed to determine levels of STYX and c-myc mRNA. Data are means \pm SD from three independent experiments.
- C HeLa cells transfected with the indicated siRNAs were lysed 72 h after transfection followed by immunoblotting against the indicated proteins.
- D, E HeLa cells were transfected with plasmids encoding STYX or with an empty vector. After 24 h, cells were treated with cycloheximide for the indicated time points followed by lysis and immunoblotting as indicated. The evaluation of three experiments is shown in (E). Asterisks indicate statistically significant differences at $P < 0.05$ (two-tailed paired *t*-test). Data are means \pm SD from three independent experiments.

Source data are available online for this figure.

pathogenic mutant of this FBP (Akhoondi *et al*, 2007; O'Neil *et al*, 2007). As substrate, we chose to test the interaction with c-myc (Yada *et al*, 2004; Welcker & Clurman, 2008). Mutation of the substrate-binding region altered the interaction with c-myc, but not with SKP1 (Fig 4A). STYX was still capable of interacting with the R456C mutant, indicating that STYX does not bind the substrate-binding region of FBXW7, which is in line with our observation that STYX is not a substrate. The F-box deletion mutant of FBXW7 was still capable of binding the substrate c-myc, but lost its ability to bind to SKP1. Intriguingly, interaction with STYX was also lost (Fig 4A), which supports our hypothesis that STYX binds FBXW7 via its F-box domain. To further substantiate this finding, we performed YFP-BiFC assays and found that the F-box deletion mutant severely lost its ability to form a complex with STYX

(Fig 4B). Furthermore, we were able to pull down STYX from cellular lysate using a purified GST-tagged F-box of FBXW7 (Appendix Fig S2). These results indicate that STYX and SKP1 might compete with binding to FBXW7. To test this experimentally, we overexpressed increasing amounts of STYX and performed co-immunoprecipitation assays between FBXW7 and SKP1. As seen in Fig 4C, the ability of FBXW7 to interact with SKP1 and CUL1 was disturbed by STYX in a dose-dependent manner. On the other hand, the ability of CUL1 to interact with SKP1 was unaffected by STYX levels (Fig 4D). Notably, the levels of FBXW7 that interacted with CUL1-SKP1 complex were reduced by increasing STYX levels. As an alternative experimental approach to test for the ability of STYX to interfere with FBXW7-SKP1 interaction, we performed fluorescence resonance energy

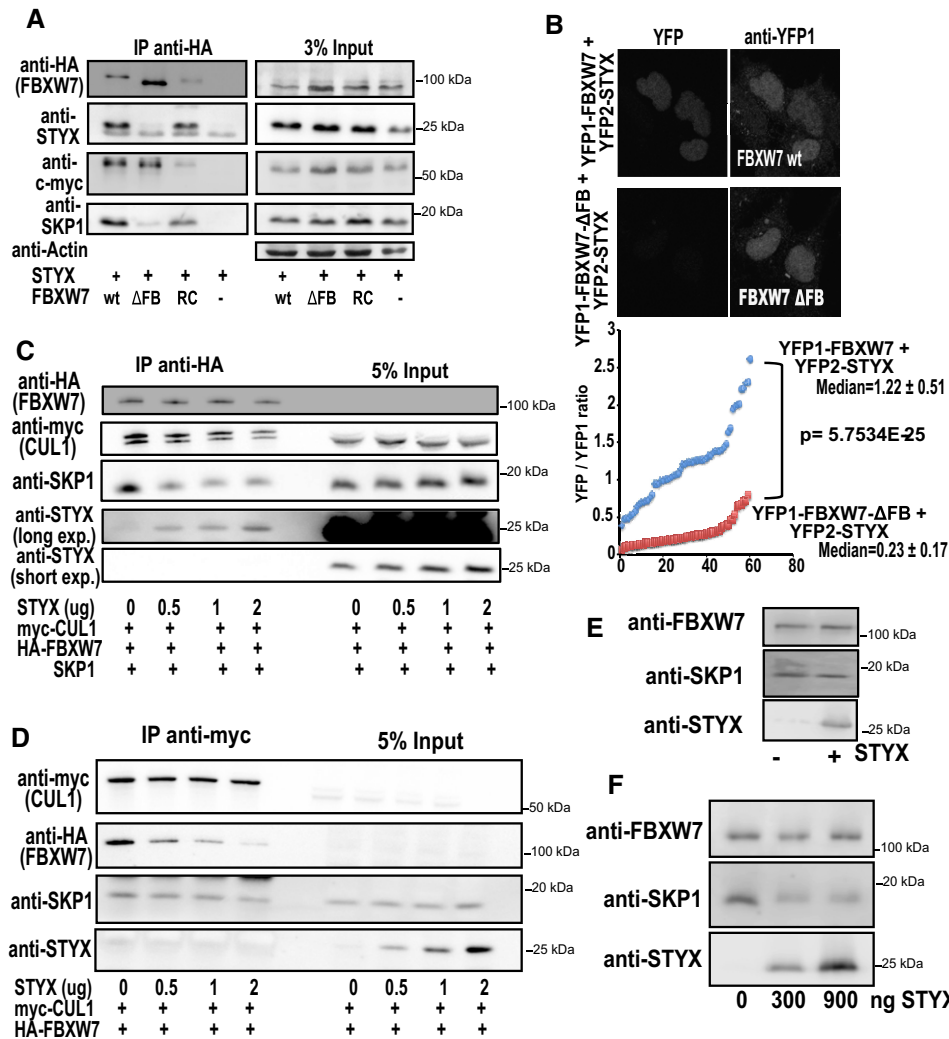


Figure 4. STYX interacts with the F-box of FBXW7.

- A** HeLa cells expressing HA-tagged wild-type FBXW7 (wt) or variants thereof lacking the F-box (ΔFB) or harboring a mutant substrate-binding domain (RC) were transfected to co-express non-tagged STYX. Cells were lysed and subjected to immunoprecipitation against HA followed by immunoblotting as indicated.
- B** YFP-BiFC between STYX and wild-type FBXW7 (WT) or a mutant lacking the F-box (ΔFB). Cells were counterstained against YFP1 (with Alexa647 secondary antibody) to control for expression levels of the YFP1-FBXW7 construct. The upper panel depicts representative cells. The lower panel shows the quantification the ratio of fluorescence intensities in the YFP-channel normalized to the YFP1 staining. Cells expressing STYX and wild-type FBXW7 are displayed as blue symbols, and cells expressing STYX and FBXW7-ΔFB are shown as red symbols. The median values are displayed next to the graph as well as the *P*-value derived from a paired Student's *t*-test.
- C, D** HeLa cells were transiently transfected with myc-tagged CUL1, HA-tagged FBXW7, non-tagged SKP1 and increasing amounts of non-tagged STYX. The amount (μg) of transfected STYX plasmid is indicated below the immunoblots. Cells were lysed and subjected to anti-HA (C) or anti-myc (D, to bring down CUL1) immunoprecipitation followed by immunoblotting against the indicated proteins.
- E** Recombinant SCF complex (0.2 μM) containing GST-tagged FBXW7 and 6xHis-tagged SKP1 was incubated with solvent (-) or with 2 μM 6xHis-tagged STYX for 30 min at 25°C followed by a GST-pulldown and immunoblotting as indicated.
- F** Recombinant GST-tagged FBXW7 (600 ng) was incubated with 300 ng of non-tagged SKP1 alone or in the presence of different doses of recombinant 6xHis-tagged STYX. The reaction was performed for 60 min at 25°C and was followed by GST-pulldown and immunoblotting as indicated.

Source data are available online for this figure.

transfer (FRET) experiments in intact cells. CFP-tagged SKP1 exhibited a robust FRET signal with YFP-tagged FBXW7. However, co-expression of STYX drastically reduced the FRET efficiency, indicating that it interferes with the FBXW7-SKP1 interaction (Appendix Fig S2B). To test whether STYX and SKP1 bind to FBXW7 in a mutually exclusive manner, we combined FRET with BiFC. The STYX-FBXW7 complex was visualized using YFP-BiFC,

which did not exhibit any appreciable FRET signal with CFP-tagged SKP1 (Appendix Fig S2B). Another prediction of our model is that a STYX immunoprecipitate should not contain SKP1. To test this experimentally, we immunoprecipitated HA-tagged STYX, CUL1, or FBXW7. SKP1 was recovered in immunoprecipitates of CUL1 and FBXW7 but not with STYX (Appendix Fig S2C), which validates the prediction of our model.

The combined results of our co-immunoprecipitation and FRET experiments lead to the question of whether STYX and SKP1 compete for binding to FBXW7, or whether STYX displaces SKP1 from FBXW7. To test for these two possible scenarios experimentally, we incubated a pre-formed SCF complex, in which SKP1 is tightly bound to FBXW7 with purified STYX. As shown in Fig 4E, STYX is not capable of displacing SKP1 when pre-bound to FBXW7. This is not surprising in light of previous observations that showed that the exchange of SKP1 out of the SCF complex is very poor and that SKP1 and FBXW7 interact very tightly and require Cand1 to break the SKP1-CUL1 interface (Pierce *et al*, 2013). Next, we tested whether STYX and SKP1 compete for binding to FBXW7. To this end, we incubated 600 ng of FBXW7 either alone with 300 ng of SKP1 or with increasing amounts of STYX. The levels of SKP1 that bound to free FBXW7 were decreased in the presence of STYX, indicating a competitive mode of interaction with FBXW7 (Fig 4F).

Altogether, these data suggest that STYX binds to the F-box domain in FBXW7 in a manner mutually exclusive with SKP1.

Identification of the domain in STYX required for the interaction with FBXW7

Because STYX is a pseudophosphatase, we asked whether its interaction with FBXW7 is dependent on its pseudoenzyme status. We mutated STYX to an active phosphatase (glycine 120 to cysteine), which we previously showed to re-gain the ability to dephosphorylate phospho-ERK2 (Reiterer *et al*, 2013). Using BiFC we found that STYX-G120C formed a complex with FBXW7 in the nucleus, in a manner undistinguishable from the wild type (Fig 5A and Appendix Fig S2D). Therefore, the pseudophosphatase domain (or the absence of catalytic activity) of STYX does not appear to mediate complex formation with FBXW7. To determine the region of STYX relevant for the interaction with FBXW7, we spotted peptides corresponding to 13-aa-long regions of STYX progressively offset by 3 aa onto a nitrocellulose membrane (Table EV2). The membrane was probed with purified GST-tagged F-box domain of FBXW7. We found that two different regions of STYX showed the strongest binding, namely ⁷⁶FQQ⁷⁸ and ¹⁴²KYR¹⁴⁴, which are located on opposing sides of the STYX molecule (Fig 5B and C; Almo *et al*, 2007). We then tested whether either of the two linear motifs is relevant for the interaction in the context of the full-length protein. We mutated the respective residues to alanine and expressed the resulting mutant STYX variants in HEK293 cells followed by co-immunoprecipitation experiments with endogenous FBXW7. Mutation of ⁷⁶FQQ⁷⁸

(hereafter termed STYX-FQQ) strongly altered the interaction with FBXW7, while mutation of ¹⁴²KYR¹⁴⁴ did not decrease binding, but appeared to increase binding (Fig 5D). We consider it unlikely that the altered interaction of STYX-FQQ with FBXW7 is due to misfolding of the mutant protein, because it localizes to the nucleus (Fig 5E) and is still capable of interacting with ERK2 (Fig 5F) in the nucleus (Fig 5G) in a manner comparable to wild-type STYX. Therefore, the STYX-FQQ mutant appears to retain the interaction with ERK2, but has an impaired interaction with FBXW7.

STYX-FBXW7 crosstalk regulates cell survival and is altered in breast cancer

FBXW7-mediated degradation of MCL1 was shown to regulate the sensitivity of cells to apoptosis (Inuzuka *et al*, 2011; Wertz *et al*, 2011). Therefore, we tested whether STYX also regulates apoptosis sensitivity. MDA-MB231 breast cancer cells stably depleted of STYX were treated with doxorubicin, and we monitored the levels of cleaved caspase-3 as an indicator of apoptosis. Knockdown of STYX markedly increased the levels of caspase-3 cleavage (Fig 6A), which is in line with our finding that STYX depletion reduced MCL1 levels in this breast cancer cell line (Appendix Fig S3A). Depletion of STYX in HeLa cells also increased apoptosis sensitivity (Appendix Fig S3B). The results of our caspase-3 cleavage experiments were supported by showing that STYX knockdown in MDA-MB231 cells increased the staining of annexin-V, a marker for apoptotic cells (Appendix Fig S3C). Knockdown of STYX also decreased the ability of MDA-MB-231 cells to form colonies under anchorage-free growth conditions (Appendix Fig S3D). This is likely due to apoptosis sensitivity, because proliferation under 2D growth conditions was not affected (data not shown). On the contrary, overexpression of STYX increased the resistance toward doxorubicin-mediated apoptosis (Fig 6B) and prevented loss of MCL1 (Fig 6B). Overexpression of the STYX-FQQ mutant that is not capable of binding FBXW7 did not exert any protection against apoptosis and did not prevent loss of MCL1 (Fig 6B), indicating that the effect of STYX on MCL1 is mediated via FBXW7. Sensitization to apoptosis by STYX knockdown was partially reversed by overexpression of MCL1 (Fig 6C). The reason for this modest effect may lie in the fact that several FBXW7 substrates regulate cell survival, but this result nevertheless suggests that the FBXW7 substrate MCL1 is an important determinant of the effect of STYX on cell death.

FBXW7 has been described as a tumor-suppressor protein (Davis *et al*, 2014; Wang *et al*, 2014), and our results so far

Figure 5. Identification of residues on STYX that mediate interaction with FBXW7.

- HeLa cells were transfected with plasmids encoding YFP1-FBXW7 together with either YFP2-tagged wild-type STYX (wt) or YFP2-tagged mutated STYX (G120C). Cells were fixed 24 h after transfection and stained against the YFP2-tag.
- 13-mer peptides of STYX shifted by 3 aa were spotted on a nitrocellulose membrane (Intavis) to cover the entire protein sequence. The membrane was probed with purified GST-tagged F-box of FBXW7 followed by immunodetection against GST. The lower panel depicts a schematic to illustrate the positions onto which the peptides were spotted (green).
- Structure of STYX (2R0B) in which the positions of the FQQ and KYR motifs are labeled using PyMol.
- Co-immunoprecipitation of endogenous FBXW7 with HA-tagged wild-type (wt) STYX or mutant versions of STYX where the KYR and FQQ motifs have been replaced by alanines.
- Representative image showing the localization of a STYX mutant where the FQQ motif has been replaced by alanines.
- Co-immunoprecipitation of Flag-tagged ERK2 with HA-tagged wild-type (wt) STYX or mutant versions of STYX where the FQQ motif has been replaced by alanines.
- YFP-BiFC between Y2-tagged wild-type (wt) STYX or the STYX-FQQ mutant and Y1-tagged ERK2 in HeLa cells. Representative cells are shown on the left side, and a quantification of average normalized YFP-fluorescence intensities is displayed on the right side. The difference between both bars is statistically not significant (two-tailed non-paired *t*-test). Data are means \pm SD from three different experiments with a minimum of 20 cells per condition per experiment.

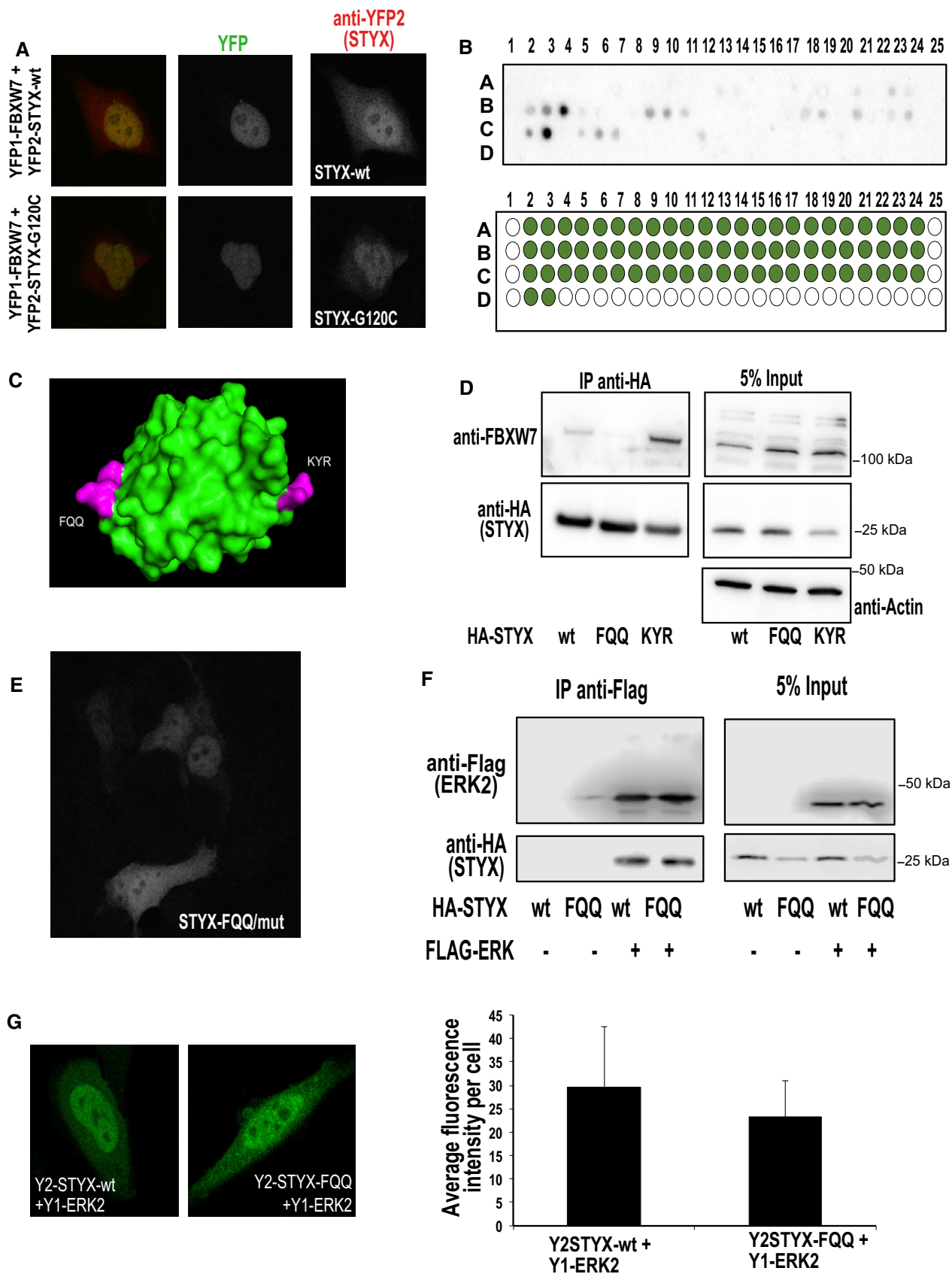


Figure 5.

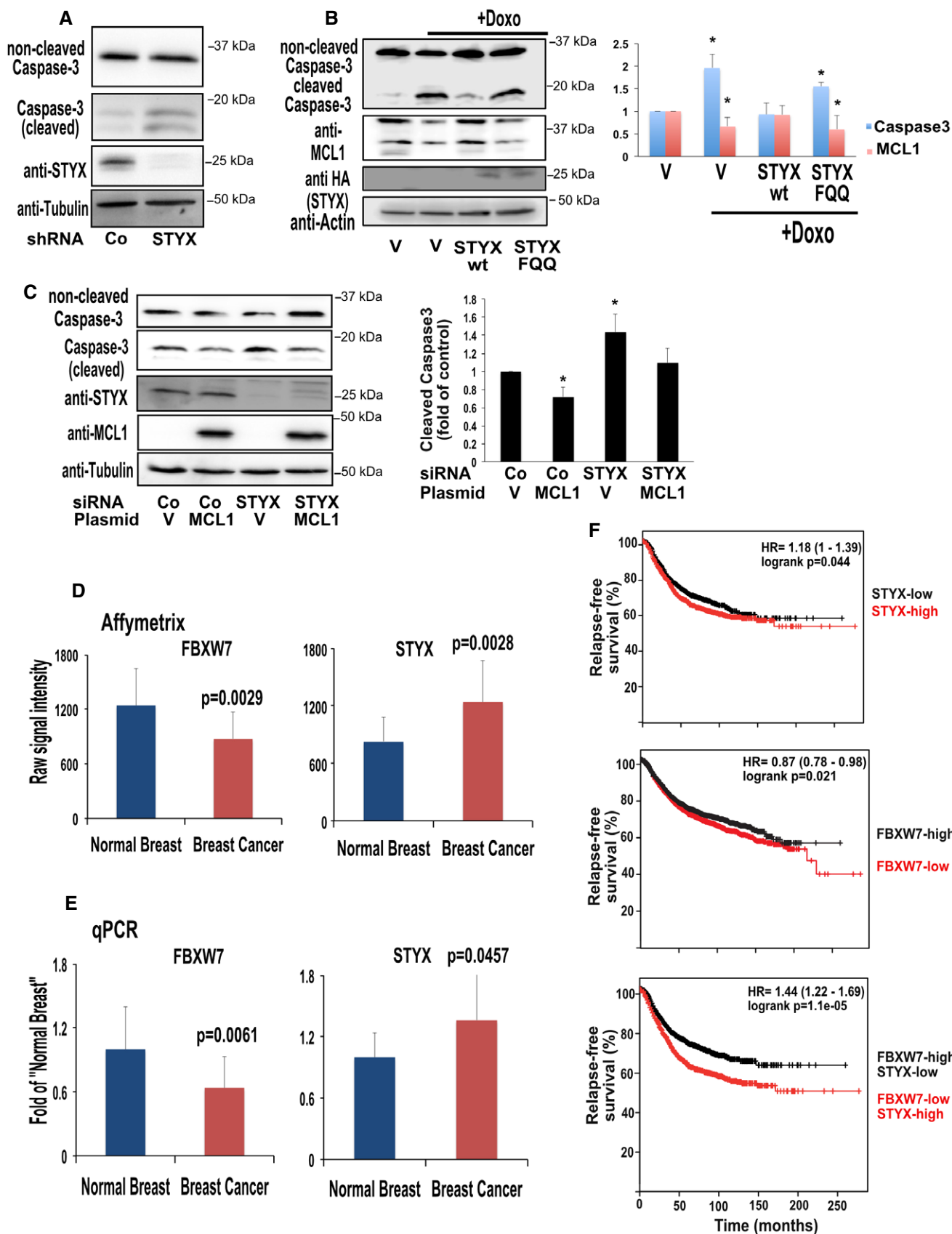


Figure 6.

Figure 6. STYX-FBXW7 crosstalk regulates apoptosis and is deregulated in cancer.

- A MDA-MB-231 stably expressing shRNA against STYX or a non-targeting control (Co) were treated with 100 μ M doxorubicin for 24 h followed by lysis and immunoblotting against the indicated proteins.
- B HeLa cells were transfected with empty vector (V) or with a plasmid encoding HA-tagged wild-type (wt) STYX or the STYX-FQQ mutant. After 24 h, cells were treated either with vehicle or with 10 μ M doxorubicin (+Doxo) for 5 h followed by lysis and immunoblotting against the indicated proteins. An evaluation of three experiments is shown on the right side of the panel. Asterisks indicate statistically significant differences tested against non-treated vector-transfected cells ($P < 0.05$; paired *t*-test). Results are means \pm SD from three independent experiments.
- C Cells transfected with the indicated siRNA were cultured for 48 h followed by transfection of an empty vector (V) or a plasmid encoding MCL1. Cells were treated with doxorubicin followed by lysis and immunoblotting as indicated. An evaluation of three experiments is shown on the left side of the panel. Asterisks indicate statistically significant differences tested against control siRNA- and vector-transfected cells ($P < 0.05$; paired *t*-test). Results are means \pm SD from three independent experiments.
- D Levels of STYX and FBXW7 in 12 non-pathologic breast samples (normal breast) and 61 breast cancers. Details of statistical tests are provided in Table EV3.
- E Levels of STYX and FBXW7 determined by qPCR analysis of nine non-pathologic mammary samples (normal breast) and 51 breast cancers. Details of statistical tests are provided in Table EV3.
- F Analysis of relapse-free survival of 1,660 breast cancer patients with the indicated alterations of gene expression.
- Source data are available online for this figure.

indicate that STYX counteracts its functions. If this were the case, we would expect these two proteins to be inversely regulated in cancer patients because this condition would confer a strong selective advantage to cancer cells. To test this hypothesis, we analyzed, using the Affymetrix GeneChip technology, the expression of STYX and FBXW7 in 12 non-pathologic breast samples and 61 breast cancers (Fig 6D; raw data in Table EV3). Indeed, the levels of STYX and FBXW7 were anti-correlated, with STYX being elevated and FBXW7 downregulated. To further validate these results, we performed qPCR analysis on those samples for which sufficient RNA was available (nine non-pathologic mammary samples and 51 breast cancers, raw data in Table EV3). We compared the levels of STYX and FBXW7 between healthy breast tissues and breast tumors and found that the levels of STYX were significantly higher in cancerous tissue compared to normal tissue while FBXW7 was downregulated in breast cancer patients (Fig 6E). Finally, we asked whether the down-regulation of FBXW7, the up-regulation of STYX, or the combination of both has an impact on the survival of breast cancer patients. We used the kmplott database (Györfy *et al*, 2010) that allows plotting the relapse-free survival (RFS) of patients with different cancers and correlate it with high or low expression of different genes. Down-regulation of FBXW7 was associated with a poor survival compared with the patient cohort with high FBXW7 levels (Fig 6F, middle), which is in line with the notion that FBXW7 is a tumor-suppressor protein. Up-regulation of STYX was also associated with a higher probability of cancer relapse (Fig 6F, top). Although both conditions had a statistically significant impact on survival, the effect was rather modest. We then combined both conditions comparing “STYX-high and FBXW7-low” with “STYX-low and FBXW7-high”. The STYX-high and FBXW7-low condition was associated with a substantially poorer prognosis than the group with the opposite expression pattern (Fig 6F, bottom). These data support the notion that STYX is a suppressor of FBXW7 and indicate that this crosstalk may be clinically relevant. We next asked whether the additive effect of STYX overexpression is specific for “FBXW7-low” patients. We analyzed a group of patients with PI3 kinase (PIK3CA) overexpression that exhibit decrease in survival and found that overexpression of STYX did not affect the survival of this group of patients to any extent (Appendix Fig S4). We described previously that loss of the Golgi matrix protein GOLGA2 alters cell polarity and might promote

tumorigenesis (Baschieri *et al*, 2014, 2015). We find that loss of GOLGA2 is associated with poorer relapse-free survival of breast cancer patients, but this is not affected to any appreciable extent by overexpression of STYX (Appendix Fig S4). Therefore, we conclude that the crosstalk of STYX and FBXW7 in cancer is specific due to the direct interaction of these two proteins.

Discussion

FBXW7 regulates a wide range of biologic processes such as cell proliferation, differentiation, and survival. In addition, it is considered a major tumor-suppressor (Welcker & Clurman, 2008; Davis *et al*, 2014; Cremona *et al*, 2016), although in few cases FBXW7 deletion was shown to be therapeutically beneficial (Busino *et al*, 2012; Takeishi *et al*, 2013). Given their biologic importance, it is conceivable that cells have evolved mechanisms to regulate the function of FBPs. In the current work, we identify the enigmatic pseudophosphatase STYX as an inhibitor of FBXW7. By binding to the F-box, STYX prevents the assembly of FBXW7 into the SCF complex, and thereby inhibits degradation of its substrates (Fig 7). Given that many of these substrates have well-known oncogenic roles, we propose that the STYX–FBXW7 interaction might represent a useful therapeutic target for future pharmacologic interventions.

With respect to FBXW7, the vast majority of regulatory mechanisms described so far are limited to the regulation of FBXW7 expression by transcriptional regulators or microRNAs (reviewed by Wang *et al*, 2014) or through the regulation of FBXW7 dimerization (Welcker & Clurman, 2007; Min *et al*, 2012; Welcker *et al*, 2013), or through the phosphorylation of its substrates. In its dimeric form, FBXW7 is trans-ubiquitylated and thereby promotes its own degradation. Another level of regulation is by phosphorylation. Protein kinase C-dependent phosphorylation of FBXW7 α was shown to control its nuclear localization (Durgan & Parker, 2010). The PI3 kinase pathway was also shown to regulate stability of FBXW7 (Schülein *et al*, 2011). The de-ubiquitinating enzymes USP28 was shown to functionally counteract FBXW7 by removing ubiquitin from the substrates of this FBP (Popov *et al*, 2007), which could explain why deletion of USP28 was found to promote colorectal cancer (Diefenbacher *et al*, 2015). On the other hand, USP28 also de-ubiquitinates FBXW7 itself and

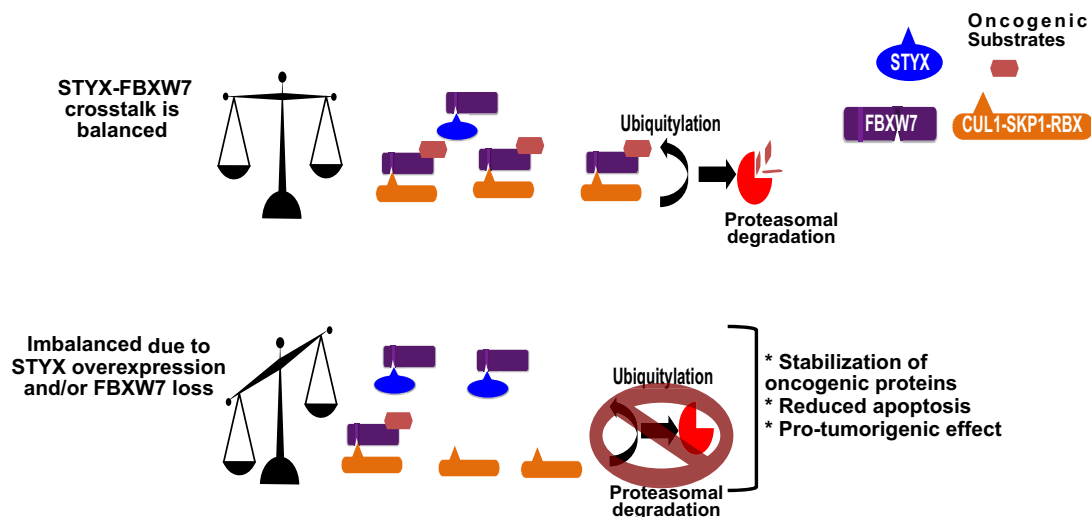


Figure 7. Model of the crosstalk between FBXW7 and STYX and its deregulation.

Under normal conditions and low STYX expression levels, FBXW7 is bound to SKP1 as well as to STYX, allowing for efficient degradation of oncogenic substrates (upper row). In breast cancer (lower row), STYX is upregulated and FBXW7 is downregulated. STYX competes with SKP1 for binding to FBXW7 and thereby inhibits the degradation of its substrates.

promotes its stabilization (Schüle-Völk *et al*, 2014). The effect of USP28 on FBXW7 is dose-dependent and therefore dependent on the relative expression levels of these proteins in different tissues.

However, FBPs act as part of an SCF complex, and therefore, it appears intuitive that they are regulated by remodeling of the architecture of SCF complexes to activate or deactivate them. The importance of targeting SCF complex assembly has been highlighted by the development of engineered ubiquitin variants that target the interfaces between SKP1, F-Box, and CUL1 (Gorelik *et al*, 2016) as well as by the fact that the broad-spectrum CRL inhibitor MLN4924 is currently being used in clinical trial (Swords *et al*, 2015). However, whether cellular proteins are capable of regulating SCF complexes has remained elusive for a long time after the discovery of SCF complexes. The first demonstration of an SCF complex regulator was made for Cand1, which was proposed to act as an exchanger of FBPs within the SCF complex (Pierce *et al*, 2013). An analogy was drawn to small GTPases where GEFs exchange GDP for GTP and thereby regulate the activity status of these proteins. In yeast, cadmium stress was shown to induce autoubiquitinylation of the F-box protein Met30, which is followed by recruitment of Cdc48 and disassembly of the SCF complex through a mechanism that remains to be determined (Yen *et al*, 2012). Whether Cdc48 competes with the interaction between the F-box and SKP1 using the mechanism that we have uncovered for STYX remains to be elucidated. Previous chemical genetics screens demonstrated that the FBP-SKP1 interaction is druggable. There, a small molecule was identified that selectively blocked the interaction of SKP1 with the FBP Met30 but not that with Cdc4 (the homolog of FBXW7) (Aghajan *et al*, 2010). A similar finding was made for SKP2 (FBXL1) (Chan *et al*, 2013). Of note, SKP2 has a pro-tumorigenic role, and thus, its pharmacologic inhibition is desired. FBXW7, on the other hand, has been mostly proposed to act as a tumor-suppressor. Thus, future efforts should be dedicated to identify strategies to block the

interaction between STYX and FBXW7 selectively. Our finding that STYX inhibits the function of FBXW7 by binding to its F-box domain tempts to consider STYX as a general inhibitor of FBPs. However, our preliminary data indicate this might not be the case, because STYX bound to FBXO31 in a manner independent from the F-box and that STYX did not interact with all FBPs that we tested and was unable to displace CUL1-SKP1 from most FBPs examined (Reiterer & Farhan, unpublished observations). Future work is needed to systematically compare the STYX-FBP interactions and to identify small molecular compounds that selectively prevent STYX from binding to FBXW7, thereby rescuing this FBP from inhibition and restoring its tumor-suppressive effects.

Materials and Methods

Cell culture, stable cell lines, and transfection

HeLa and HEK293 cells were cultured in DMEM (GIBCO) supplemented with 10% FCS and 1% penicillin/streptomycin. HCT116, HCT116^{FBXW7-/-} cells (obtained from Horizon), and MDA-MB231 cells were cultured in RPMI supplemented with 10% FCS and 1% penicillin/streptomycin.

To establish stable cell lines, MDA-MB231 cells were infected with a lentivirus encoding an empty lentiviral vector (pVLTHM) or a vector encoding an shRNA against STYX (V2LHS_148734, Thermo Scientific). The transduced cells were selected using puromycin.

Transfection

For knockdown experiments cells were seeded into 6-well plates and reverse transfected with 5–10 nM siRNA and HiPerfect (Qiagen) according to the manufacturer's instructions. Cells were harvested 72 h after transfection. The following siRNAs were used in this study: siRNA against STYX from Qiagen (SI05391330), siRNA

against STYX from Dharmacon (L-009571-00-0005), and siRNA against FBXW7 from Dharmacon (L-009571-00-0005).

For overexpression experiments, cells were seeded into 6-well plates or 10-cm dishes. 24 h later, cells were transfected with 1–2 µg plasmid DNA (6-well plates) or 2–3 µg of each plasmid for a 10-cm dish. TransIT[®]-LT1 (Mirus) was used as a transfection reagent according to the manufacturer's instructions. Cells were harvested 24 h after transfection.

Immunoprecipitation, protein extraction and immunoblotting

Immunoprecipitation

Cells were seeded into 10-cm dishes and transfected as described above. 24 h after transfection, cells were washed twice with ice-cold PBS and lysed in 500 µl buffer (50 mM Tris-HCl pH 7.4; 10% glycerol, 150 mM NaCl, 2 mM EDTA, 0.5% Triton X-100) supplemented with proteinase inhibitors (cOmplete[™] Protease Inhibitor Cocktail Roche) and phosphatase inhibitors (PhosSTOP[™], Roche). Lysates were incubated on ice for 30 min, subsequently centrifuged at 4°C at 20,000 g for 20 min. Supernatant was transferred into a fresh tube and 3–5% was removed to serve as input for the immunoprecipitation. Immunoprecipitations against HA-tag or Flag-tag were performed using anti-HA-agarose (Sigma) or ANTI-FLAG[®] M2 Affinity Gel, respectively. In all conditions, the beads were added to the lysates and incubated end-over-end shaking overnight at 4°C. Subsequently, beads were washed four times with IP buffer and eluted in 5× reducing loading buffer by boiling for 3 min. Samples were loaded on SDS-polyacrylamide gels or on NuPAGE[™] Novex[™] 4–12% Bis-Tris Protein Gels (Thermo Fisher Scientific) and blotted on nitrocellulose membrane using semidry transfer. The membrane was blocked with either 5% milk in TBS-Tween 0.1% (TBST; 20 mM Tris, 150 mM NaCl, pH 7.6, 0.1% Tween-20) or in Rotiblock (Roth) for 1 h. Subsequently, the membrane was incubated with the first antibody 2 h at room temperature of overnight at 4°C, washed with TBST, and incubated with the secondary antibody in 5% milk in TBST for 1 h at room temperature. Membranes were washed and developed with Clarity[™] Western ECL (Bio-Rad), and the signal was detected using the ChemiDoc MP (Bio-Rad) imaging system.

Antibodies

A list of antibodies used in this study is shown in Appendix Table S1.

Immunofluorescence and confocal microscopy

Cells were seeded on glass coverslips and 24 h later transfected with the indicated plasmids. 24 h after, transfection cells were fixed with 4% paraformaldehyde for 20 min at room temperature. Cells were washed four times in PBS supplemented with 20 mM glycine and permeabilized. In the case of anti-YFP2 staining, cells were permeabilized in PBS with 0.5% Triton X-100 for 5 min at room temperature. In the case of YFP1 staining, the permeabilization buffer contained: PBS, 0.2% Triton X-100, 4% BSA, 0.5% SDS for 10 min at room temperature. Cells were incubated with primary antibody in PBS with 3% BSA and 20 mM glycine for 1 h at room temperature (for anti-Flag and anti-YFP2 staining) or overnight at 4°C (for anti-YFP1 staining). Afterward, cells were washed and incubated with the appropriate fluorescently labeled secondary antibody for

1 h at room temperature. Cells were embedded in mounting medium (polyvinyl alcohol mounting medium with DABCO, Sigma-Aldrich) and visualized using a Leica SP5 confocal microscope.

Protein purification and peptide array

Protein purification

Arctic bacteria were transformed with a plasmid encoding for GST-Fbox^{FBXW7}. An overnight culture was grown at 37°C in 50 ml HSG medium (13.5 g/l peptone, 7 g/l yeast extract, 14.9 g/l glycerol, 2.5 g/l NaCl, 2.3 g/l K₂HPO₄, 1.5 g/l KH₂PO₄, 0.14 g/l MgSO₄). The overnight culture was diluted to 0.1 OD₆₀₀, and the culture was grown for 3 h at 37°C. Subsequently, the expression of fusion proteins was induced with isopropyl-1-thio-β-D-galactopyranoside (0.5 mM) for 24 h at 10°C. Afterward bacteria were pelleted, resuspended in PBS supplemented with proteinase inhibitor, and disrupted with a cell disruptor (2 × 2.5 kbar). The lysate was cleared by centrifugation (12,000 g, 4°C, 30 min). The supernatant was incubated with Glutathione Sepharose 4 Fast Flow (GE Healthcare) for 2 h at 4°C, washed three times, and the protein was eluted in 5 mM glutathione in PBS. The buffer was exchanged to 50 mM Tris-HCl, pH 7.5, 150 mM NaCl, 5% glycerol using PD-10 Desalting Columns (GE Healthcare).

Peptide array

A customized array of overlapping 13 amino acid STYX peptides sliding 3 aa with each following peptide spotted on a modified cellulose membrane was obtained from Intavis (membrane loading 400 nm/cm²). The membrane was wetted with methanol and subsequently washed with Tris-buffered saline (TBS) (50 mM Tris, pH 7, 137 mM NaCl, 2.7 mM KCl) and subsequently blocked with membrane blocking solution (MBS) overnight (casein blocking buffer (Sigma) in T-TBS (TBS with 0.05% Tween-20), 146 mM sucrose). Afterward the membrane was washed with TBS and incubated with 5 µg/ml GST-Fbox^{FBXW7} protein in MBS for 4 h, washed with T-TBS, incubated with GST antibody in MBS overnight. The membrane was washed with T-TBS and incubated with the HRP-conjugated secondary antibody for 2 h in MBS. Subsequently, the membrane was washed twice with T-TBS and once with TBS, incubated with ECL and the resulting signal was visualized with a digital imager.

GST-pulldown

Three hundred nanograms of GST-FBXW7 (Abnova) was bound to GSH-Sepharose in PBS supplemented with 1 mM DTT and proteinase inhibitor overnight. Subsequently, beads were blocked with 5% BSA in PBS for 2 h and incubated with 300 ng purified His-tagged STYX (Abcam) for 2 h. GSH-Sepharose was washed three times with PBS supplemented with 0.5% NP-40 and once with PBS. Proteins were eluted by boiling in 5× reducing loading buffer for 3 min and subjected to SDS-PAGE.

Displacement assay

For displacement assays, SCF complex containing GST-tagged FBXW7 (Millipore, #23-030) at a final concentration of 0.2 µM was incubated with 2 µM 6xHis-tagged STYX (from Abcam) in

buffer (130 mM NaCl, 15% glycerol, 40 mM Tris pH 8) for 30 min at 25°C. The reaction was stopped by transfer to ice followed by GST-pulldown and immunoblotting.

Competition assay

Each reaction was performed in a volume of 30 μ l. Six hundred nanograms of recombinant GST-tagged FBXW7 (from Abnova) was bound to GSH-Sepharose and incubated with 300 ng of non-tagged SKP1 (from Fitzgerald) alone or in the presence of different amounts of recombinant 6xHis-tagged STYX (from Abcam). The reaction was performed for 60 min at 25°C in binding buffer (25 mM Tris-HCl, 120 mM NaCl, 9% glycerol). Subsequently, the tubes were transferred to ice for 5 min followed by centrifugation at 500 g for 5 min. After washing for three times in binding buffer, beads were boiled in sample buffer and the eluate was subjected to SDS-PAGE.

Mass spectrometry

Eluted immune complexes were precipitated with trichloroacetic acid (Sigma-Aldrich) followed by digestion with trypsin (Promega) and desalting by StageTips essentially as previously described (Behrends *et al*, 2010). Peptide samples were separated on a nano-flow HPLC system (Thermo Scientific) and analyzed on a LTQ Velos or LTQ Orbitrap Elite (Thermo Scientific). Spectra were identified by Sequest searches followed by target-decoy filtering and linear discriminant analysis as described in Huttlin *et al* (2010). Peptides that could be assigned to more than one protein in the database were assembled into proteins according to parsimony principles. For CompPASS analysis, we employed 98 unrelated bait proteins that were all previously processed in the same way (Sowa *et al*, 2009). Normalized and weighted D scores (WDN scores) were calculated based on average peptide spectral matches (APSMs). Proteins with NWD ≥ 1 and APSM ≥ 2 were considered as HCIPs.

Expanded View for this article is available online.

Acknowledgements

We thank Markus Welcker, Bruce Clurman, Anne-Claude Gingras, Melanie Cobb, and Nikita Popov for providing different plasmids for FBXW7, CUL1, SKP1. We thank Alexander Krämer, Alexander Keller and Nicola Catone and Annette Aichem for technical help. H.F. is supported by the German Science Foundation (DFG), by the Canton of Thurgau, by the Swiss Science Foundation and by the Young Scholar Fund of the University of Konstanz. C.B. is supported by the LOEWE Program (Ub-Net) of the State of Hessen (Germany) and the European Research Council (282333-XABA). P.P.D.F. is supported by Associazione Italiana per la Ricerca sul Cancro (AIRC—IG 14404 to PPDF and MCO 10.000), Italian Ministry of Health, Monzino Foundation.

Author contributions

VR performed and analyzed experiments; CF-P performed experiments; FLG performed mass spectrometry experiments; SC and MV performed Affymetrix and qPCR experiments and analyzed the data from breast cancer patients; PPDF analyzed breast cancer data; SMK and DJ performed and analyzed mass spectrometry experiments; RJD analyzed data and provided reagents; CB analyzed mass spectrometry experiments and contributed to the overall study design; HF

conceived the project, analyzed the data, and supervised the study; and VR, SC, MV, PPDF, RJD, CB, and HF wrote the manuscript.

Conflict of interest

The authors declare that they have no conflict of interest.

References

- Aghajani M, Jonai N, Flick K, Fu F, Luo M, Cai X, Ouni I, Pierce N, Tang X, Lomenick B, Damoiseaux R, Hao R, Del Moral PM, Verma R, Li Y, Li C, Houk KN, Jung ME, Zheng N, Huang L *et al* (2010) Chemical genetics screen for enhancers of rapamycin identifies a specific inhibitor of an SCF family E3 ubiquitin ligase. *Nat Biotechnol* 28: 738–742
- Akhoondi S, Sun D, von der Lehr N, Apostolidou S, Klotz K, Maljukova A, Cepeda D, Fiegl H, Dafou D, Marth C, Mueller-Holzner E, Corcoran M, Dagnell M, Nejad SZ, Nayer BN, Zali MR, Hansson J, Egyhazi S, Petersson F, Sangfelt P *et al* (2007) FBXW7/hCDC4 is a general tumor suppressor in human cancer. *Cancer Res* 67: 9006–9012
- Almo SC, Bonanno JB, Sauder JM, Emtage S, Dilorenzo TP, Malashkevich V, Wasserman SR, Swaminathan S, Eswaramoorthy S, Agarwal R, Kumaran D, Madegowda M, Ragumani S, Patskovsky Y, Alvarado J, Ramagopal UA, Faber-Barata J, Chance MR, Sali A, Fiser A *et al* (2007) Structural genomics of protein phosphatases. *J Struct Funct Genomics* 8: 121–140
- Baschieri F, Confalonieri S, Bertalot G, Di Fiore PP, Dietmaier W, Leist M, Crespo P, Macara IG, Farhan H (2014) Spatial control of Cdc42 signalling by a GM130-RasGRF complex regulates polarity and tumorigenesis. *Nat Commun* 5: 4839
- Baschieri F, Uetz-von Allmen E, Legler DF, Farhan H (2015) Loss of GM130 in breast cancer cells and its effects on cell migration, invasion and polarity. *Cell Cycle* 14: 1139–1147
- Behrends C, Sowa ME, Gygi SP, Harper JW (2010) Network organization of the human autophagy system. *Nature* 466: 68–76
- Busino L, Millman SE, Scotto L, Kyrtatous CA, Basrur V, O'Connor O, Hoffmann A, Elenitoba-Johnson KS, Pagano M (2012) Fbxw7 α - and GSK3-mediated degradation of p100 is a pro-survival mechanism in multiple myeloma. *Nat Cell Biol* 14: 375–385
- Chan CH, Morrow JK, Li CF, Gao Y, Jin G, Moten A, Stagg LJ, Ladbury JE, Cai Z, Xu D, Logothetis CJ, Hung MC, Zhang S, Lin HK (2013) Pharmacological inactivation of Skp2 SCF ubiquitin ligase restricts cancer stem cell traits and cancer progression. *Cell* 154: 556–568
- Cremona CA, Sancho R, Diefenbacher ME, Behrens A (2016) Fbw7 and its counteracting forces in stem cells and cancer: oncoproteins in the balance. *Semin Cancer Biol* 36: 52–61
- Davis RJ, Welcker M, Clurman BE (2014) Tumor suppression by the Fbw7 ubiquitin ligase: mechanisms and opportunities. *Cancer Cell* 26: 455–464
- Diefenbacher ME, Chakraborty A, Blake SM, Mitter R, Popov N, Eilers M, Behrens A (2015) Usp28 counteracts Fbw7 in intestinal homeostasis and cancer. *Cancer Res* 75: 1181–1186
- Durgan J, Parker PJ (2010) Regulation of the tumour suppressor Fbw7 α by PKC-dependent phosphorylation and cancer-associated mutations. *Biochem J* 432: 77–87
- Gorelik M, Orlicky S, Sartori MA, Tang X, Marcon E, Kurinov I, Greenblatt JF, Tyers M, Moffat J, Sicheri F, Sidhu SS (2016) Inhibition of SCF ubiquitin ligases by engineered ubiquitin variants that target the Cul1 binding site on the Skp1-F-box interface. *Proc Natl Acad Sci USA* 113: 3527–3532

- Györfy B, Lanczky A, Eklund AC, Denkert C, Budczies J, Li Q, Szallasi Z (2010) An online survival analysis tool to rapidly assess the effect of 22,277 genes on breast cancer prognosis using microarray data of 1,809 patients. *Breast Cancer Res Treat* 123: 725–731
- Huttlin EL, Jedrychowski MP, Elias JE, Goswami T, Rad R, Beausoleil SA, Villén J, Haas W, Sowa ME, Gygi SP (2010) A tissue-specific atlas of mouse protein phosphorylation and expression. *Cell* 143: 1174–1189
- Inuzuka H, Shaik S, Onoyama I, Gao D, Tseng A, Maser RS, Zhai B, Wan L, Gutierrez A, Lau AW, Xiao Y, Christie AL, Aster J, Settleman J, Gygi SP, Kung AL, Look T, Nakayama KI, DePinho RA, Wei W (2011) SCF(FBW7) regulates cellular apoptosis by targeting MCL1 for ubiquitylation and destruction. *Nature* 471: 104–109
- Jin J, Cardozo T, Lovering RC, Elledge SJ, Pagano M, Harper JW (2004) Systematic analysis and nomenclature of mammalian F-box proteins. *Genes Dev* 18: 2573–2580
- Koepp DM, Schaefer LK, Ye X, Keyomarsi K, Chu C, Harper JW, Elledge SJ (2001) Phosphorylation-dependent ubiquitination of cyclin E by the SCFFbw7 ubiquitin ligase. *Science* 294: 173–177
- Mao JH, Kim IJ, Wu D, Climent J, Kang HC, DelRosario R, Balmain A (2008) FBXW7 targets mTOR for degradation and cooperates with PTEN in tumor suppression. *Science* 231: 1499–1502
- Min SH, Lau AW, Lee TH, Inuzuka H, Wei S, Huang P, Shaik S, Lee DY, Finn G, Balastik M, Chen CH, Luo M, Tron AE, Decaprio JA, Zhou XZ, Wei W, Lu KP (2012) Negative regulation of the stability and tumor suppressor function of Fbw7 by the Pin1 prolyl isomerase. *Mol Cell* 46: 771–783
- Oberg C, Li J, Pauley A, Wolf E, Gurney M, Lendahl U (2001) The Notch intracellular domain is ubiquitinated and negatively regulated by the mammalian Sel-10 homolog. *J Biol Chem* 276: 35847–35853
- O’Neil J, Grim J, Strack P, Rao S, Tibbitts D, Winter C, Hardwick J, Welcker M, Meijerink JP, Pieters R (2007) FBW7 mutations in leukemic cells mediate NOTCH pathway activation and resistance to gamma-secretase inhibitors. *J Exp Med* 204: 1813–1824
- Petroski MD, Deshaies RJ (2005) Function and regulation of cullin-RING ubiquitin ligases. *Nat Rev Mol Cell Biol* 6: 9–20
- Pierce NW, Lee JE, Liu X, Sweredoski MJ, Graham RL, Larimore EA, Rome M, Zheng N, Clurman BE, Hess S, Shan SO, Deshaies RJ (2013) Cand1 promotes assembly of new SCF complexes through dynamic exchange of F box proteins. *Cell* 153: 206–215
- Popov N, Wanzel M, Madiredjo M, Zhang D, Beijersbergen R, Bernards R, Moll R, Elledge SJ, Eilers M (2007) The ubiquitin-specific protease USP28 is required for MYC stability. *Nat Cell Biol* 9: 765–774
- Reiterer V, Fey D, Kolch W, Kholodenko BN, Farhan H (2013) Pseudophosphatase STYX modulates cell-fate decisions and cell migration by spatiotemporal regulation of ERK1/2. *Proc Natl Acad Sci USA* 110: E2934–E2943
- Reiterer V, Eyers PA, Farhan H (2014) Day of the dead: pseudokinases and pseudophosphatases in physiology and disease. *Trends Cell Biol* 24: 489–505
- Schülein C, Eilers M, Popov N (2011) PI3K-dependent phosphorylation of Fbw7 modulates substrate degradation and activity. *FEBS Lett* 585: 2151–2157
- Schülein-Völk C, Wolf E, Zhu J, Xu W, Taranets LM, Hellmann A, Jänicke LA, Diefenbacher ME, Behrens A, Eilers M, Popov N (2014) Dual regulation of Fbw7 function and oncogenic transformation by Usp28. *Cell Rep* 9: 1099–1109
- Sowa ME, Bennett EJ, Gygi SP, Harper JW (2009) Defining the human deubiquitinating enzyme interaction landscape. *Cell* 138: 389–403
- Strohmaier H, Spruck CH, Kaiser P, Won KA, Sangfelt O, Reed SI (2001) Human F-box protein hCdc4 targets cyclin E for proteolysis and is mutated in a breast cancer cell line. *Nature* 413: 310–322
- Swords RT, Erba HP, DeAngelo DJ, Bixby DL, Altman JK, Maris M, Hua Z, Blakemore SJ, Faessel H, Sedarati F, Dezube BJ, Giles FJ, Medeiros BC (2015) Pevonedistat (MLN4924), a First-in-Class NEDD8-activating enzyme inhibitor, in patients with acute myeloid leukaemia and myelodysplastic syndromes: a phase 1 study. *Br J Haematol* 169: 534–543
- Takeishi S, Matsumoto A, Onoyama I, Naka K, Hirao A, Nakayama KI (2013) Ablation of Fbxw7 eliminates leukemia-initiating cells by preventing quiescence. *Cancer Cell* 23: 347–361
- Tan MK, Lim HJ, Bennett EJ, Shi Y, Harper JW (2013) Parallel SCF adaptor capture proteomics reveals a role for SCFFBXL17 in NRF2 activation via BACH1 repressor turnover. *Mol Cell* 52: 9–24
- Wang L, Ye X, Liu Y, Wei W, Wang Z (2014) Aberrant regulation of FBW7 in cancer. *Oncotarget* 5: 2000–2015
- Welcker M, Orian A, Jin J, Grim JE, Harper JW, Eisenman RN, Clurman BE (2004) The Fbw7 tumor suppressor regulates glycogen synthase kinase 3 phosphorylation-dependent c-Myc protein degradation. *Proc Natl Acad Sci USA* 101: 9085–9090
- Welcker M, Clurman BE (2007) Fbw7/hCDC4 dimerization regulates its substrate interactions. *Cell Div* 2: 7
- Welcker M, Clurman BE (2008) FBW7 ubiquitin ligase: a tumour suppressor at the crossroads of cell division, growth and differentiation. *Nat Rev Cancer* 8: 83–93
- Welcker M, Larimore EA, Swanger J, Bengoechea-Alonso MT, Grim JE, Ericsson J, Zheng N, Clurman BE (2013) Fbw7 dimerization determines the specificity and robustness of substrate degradation. *Genes Dev* 27: 2531–2536
- Wertz IE, Kusam S, Lam C, Okamoto T, Sandoval W, Anderson DJ, Helgason E, Ernst JA, Eby M, Liu J, Belmont LD, Kaminker JS, O’Rourke KM, Pujara K, Kohli PB, Johnson AR, Chiu ML, Lill JR, Jackson PK, Fairbrother WJ (2011) Sensitivity to antitubulin chemotherapeutics is regulated by MCL1 and FBW7. *Nature* 471: 110–114
- Wishart MJ, Dixon JE (1998) Gathering STYX: phosphatase-like form predicts functions for unique protein-interaction domains. *Trends Biochem Sci* 23: 301–306
- Yada M, Hatakeyama S, Kamura T, Nishiyama M, Tsunematsu R, Imaki H, Ishida N, Okumura F, Nakayama K, Nakayama KI (2004) Phosphorylation-dependent degradation of c-Myc is mediated by the F-box protein Fbw7. *EMBO J* 23: 2116–2125
- Yen JL, Flick K, Papagiannis CV, Mathur R, Tyrrell A, Ouni I, Kaake RM, Huang L, Kaiser P (2012) Signal-induced disassembly of the SCF ubiquitin ligase complex by Cdc48/p97. *Mol Cell* 48: 288–297
- Zhao D, Zheng HQ, Zhou Z, Chen C (2010) The Fbw7 tumor suppressor targets KLF5 for ubiquitin-mediated degradation and suppresses breast cell proliferation. *Cancer Res* 70: 4728–4738